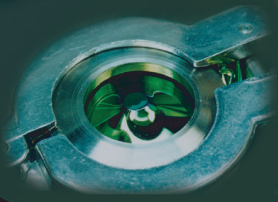
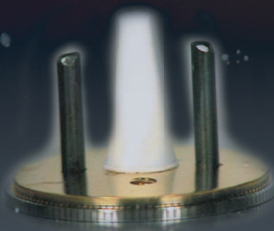
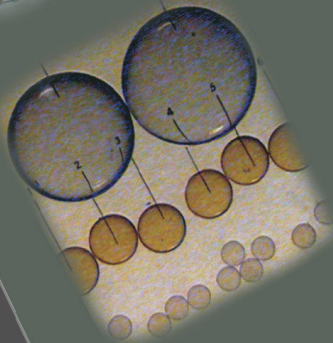
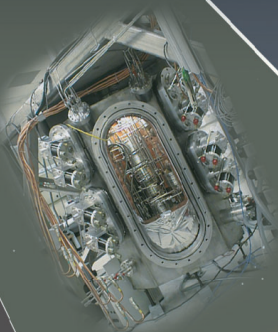
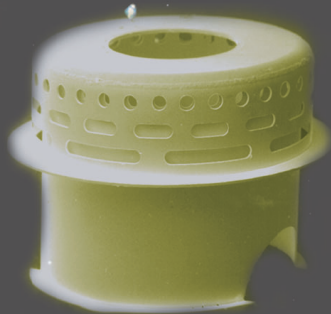


Inertial Confinement Fusion

ANNUAL REPORT

OCTOBER 1, 2000
THROUGH
SEPTEMBER 30, 2001



The artwork on the front cover shows samples of the target components and systems GA has developed and fabricated as part of our role as ICF Target Support contractor. Shown are the ICF Program's experiments and examples of things we have provided for these experiments:

Clockwise from the top:

1. The target chamber of the Nike Laser at the Naval Research Laboratory, with planar targets on a Nike Target Mount (vertical) and a Cryogenic Target Mount (horizontal).
2. The Z machine in action at Sandia National Laboratories, Albuquerque, with a foam cone target and a foam target shell.
3. Inside the OMEGA Laser's target chamber at University of Rochester/Laboratory for Laser Energetics, with a variety of plastic capsules for direct and indirect drive experiments, and a view of the OMEGA Cryogenic Target System.
4. The National Ignition Facility Target System target chamber with half a cryogenic hohlraum and a prototype cryogenic parting joint for the NIF Cryogenic Target System.

DISCLAIMER

This report was prepared as an account of work sponsored by an agency of the United States Government. Neither the United States Government nor any agency thereof, nor any of their employees, makes any warranty, express or implied, or assumes any legal liability or responsibility for the accuracy, completeness, or usefulness of any information, apparatus, product, or process disclosed, or represents that its use would not infringe privately owned rights. Reference herein to any specific commercial product, process, or service by trade name, trademark, manufacturer, or otherwise, does not necessarily constitute or imply its endorsement, recommendation, or favoring by the United States Government or any agency thereof. The views and opinions of authors expressed herein do not necessarily state or reflect those of the United States Government or any agency thereof.

GA-A23852

**INERTIAL CONFINEMENT FUSION
TARGET COMPONENT FABRICATION AND
TECHNOLOGY DEVELOPMENT SUPPORT**

**ANNUAL REPORT TO THE
U.S. DEPARTMENT OF ENERGY**

OCTOBER 1, 2000 THROUGH SEPTEMBER 30, 2001

**by
PROJECT STAFF**

W.J. Miller, Editor

**Work prepared under
Department of Energy
Contract Nos. DE-AC03-01SF22260
and DE-AC03-95SF20732**

**GENERAL ATOMICS PROJECTS 03748 and 30095
DATE PUBLISHED: APRIL 2001**



ACRONYMS

AES	Auger electron spectroscopic
AFM	atomic force microscope
CD ₄	deuterated methane
CPL	cryogenic pressure loader
CRF	carbonized resorcinol-formaldehyde
CTARPOS	Cryogenic TARget POSitioner
CTM	cryogenic target mount
D ₂ TS	deuterium test system
DT	deuterium-tritium
DVB	divinyl benzene
EDAX	energy dispersive x-ray analysis
EOS	equation of state
FTIR	Fourier Transform Infrared
FWHM	full width half maximum
GDP	glow discharge polymer
GA	General Atomics
HD	hydrogen deuteride
HIRC	Hydrogen Isotopes Research Center
ICF	Inertial Confinement Fusion
IDL™	Interactive Data Language
IFE	Inertial Fusion Energy
IFT	Inertial Fusion Technology
IR	infrared
LANL	Los Alamos National Laboratory
LCS	local control system
LEH	laser entrance hole
LLNL	Lawrence Livermore National Laboratory

LVDT	linear variable differential transformers
NCTS	NIF Cryogenic Target System
NIF	National Ignition Facility
NNSA	National Nuclear Security Administration
NRL	Naval Research Laboratory
OCTHS	OMEGA Cryogenic Target Handling System
PAA	polyacrylic acid
PAMS	poly(α -methylstyrene)
PCHMS	polycyclohexylmethylsilylene C ₇ H ₁₄ Si
PMDA	pyromellitic dianhydride
PS	polystyrene
PSF	point spread function
PVA	polyvinyl alcohol
RF	resorcinol-formaldehyde
SEM	scanning electron microscope
Si-GDP	silicon-doped glow discharge polymer
SNL	Sandia National Laboratory
TARPOS	TARget POSitioner
TIC	target insertion cryostats
TPX	commercial designation of the polymer produced by the polymerization of 4-methylpentene-1
UR/LLE	University of Rochester/Laboratory for Laser Energetics
UV	ultraviolet
WBS	work breakdown structure
WETF	Weapons Engineering Tritium Facility
XRF	x-ray fluorescence

TABLE OF CONTENTS

1. EXECUTIVE SUMMARY	1-1
2. INTRODUCTION	2-1
3. PROGRAM ACCOMPLISHMENTS	3-1
3.1. Program Overview	3-1
3.2. Advanced Technology and Cryogenics Excellence	3-2
3.2.1. The Deuterium Test System (N. Alexander)	3-2
3.2.2. NIF Cryogenic Target System Development and Engineering (N. Alexander).....	3-4
3.2.3. Design of the Beryllium Capsule DT Fill Station (C. Gibson)	3-10
3.3. Polymer and Coatings Developments	3-14
3.3.1. UR/LLE Deliveries (A. Nikroo).....	3-14
3.3.2. PAMS Shells (F. Elsner)	3-18
3.3.3. Stronger, Denser GDP Shells for OMEGA and NIF (A. Nikroo)	3-21
3.3.4. Composition and Aging Studies of Strong and “Normal” GDP (D. Czechowicz)	3-26
3.3.5. Polyimide Coater Development (A. Nikroo)	3-29
3.4. Inertial Fusion Capsule Production	3-32
3.4.1. LLNL, LANL, and SNL Capsule Deliveries (A. Greenwood)	3-32
3.4.2. Glass Shells from Doped GDP (M. Hoppe)	3-40
3.4.3. PVA Coating Improvements (D. Steinman)	3-46
3.4.4. Polishing Beryllium Shells (M. Hoppe)	3-49
3.5. Target Component Fabrication and Fabrication Development	3-52
3.5.1. LLNL, LANL, and SNL Deliveries (J. Kaae)	3-52
3.5.2. Roughened Hohlräum Surfaces (J. Smith)	3-55
3.5.3. Specialized Planar Components (J. Smith)	3-58
3.6. Schafer Activities	3-61
3.6.1. Operations (K. Shillito)	3-61
3.6.2. Inertial Fusion Foam Target Development and Production (D. Schroen)	3-65

3.6.3. Advanced Planar Targets (T. Walsh)	3-73
3.6.4. Advanced Cryogenic Layering and Engineering Development (J. Sater)	3-83
3.7. Operations	3-94
3.7.1. On-Site Support at LLNL (W. Miller)	3-95
3.7.2. Cryogenic Pressure Loader Development and Research at LANL (J. Sheliak)	3-97
3.8. Characterization Innovation and Development	3-108
3.8.1. NIF Indirect Drive Target Characterization Requirements (R. Stephens)	3-108
3.8.2. Improvements in the Spheremapper and Wallmapper (R. Stephens)	3-110
3.8.3. Thickness and Uniformity of Thin Gold Layers (A. Greenwood)	3-111
4. ORGANIZATION	4-1
4.1. Introduction	4-1
4.2. Structure	4-1
4.3. Centers	4-3
4.3.1. Program Management	4-3
4.3.2. Center for Advanced Technology and Cryogenics Excellence	4-5
4.3.3. Center for Polymer and Coatings Developments	4-7
4.3.4. Center for Inertial Fusion Capsule Production	4-10
4.3.5. Center for Target Component Fabrication and Fabrication Development	4-13
4.3.6. Schafer Activities	4-15
4.3.7. Operations Office	4-23
4.3.8. Characterization Innovation and Development Office	4-25
5. PUBLICATIONS	5-1
5.1. List of Publications	5-1
5.2. List of Presentations	5-3
5.3. Invited Talks	5-9
5.4. Awards	5-9
6. ACKNOWLEDGEMENT	6-1

LIST OF FIGURES

1-1.	The GA/Schafer inertial confinement technology team expertise ...	1-1
2-1.	GA/Schafer capsule implosion target design timeline	2-2
3-1.	The assembly layout of the D ₂ TS	3-3
3-2.	Filled targets will be moved from the bellows assembly into the main cryostat	3-3
3-3.	The main cryostat maintained a surrogate target temperature	3-4
3-4.	The permeation cell for a system nearly identical to that of D ₂ TS	3-5
3-5.	The NCTS will take a target	3-6
3-6.	The WBS for the Target Cryostats System	3-6
3-7.	The TIC hexapod attached to the helium tank positions the TIC nose cone and the target held in the gripper	3-7
3-8.	The indirect drive target gripper	3-8
3-9.	In the direct drive TIC, the positioner stages used to locate the target in the shroud are located in the mechanisms bay	3-9
3-10.	Baseline design of the NIF DD Polymer Fill System	3-10
3-11.	The DT Compression System and Be Capsule Fill Station	3-11
3-12.	Inner components of the Be Capsule Fill Station	3-12
3-13.	In the decomposable mandrel technique, a PAMS shell is coated with the plasma GDP	3-15
3-14.	An example of a set of targets requiring layers of GDP and D -GDP	3-15
3-15.	An example of a set of targets requiring layers of GDP and Ti -GDP	3-16
3-16.	Completion of UR/LLE request for multiple layer GDP shells	3-17
3-17.	This figure shows the diameter range of many of the capsules delivered to UR/LLE in FY01	3-17
3-18.	The inventory of PAMS shells was built up over a broad range of sizes	3-18
3-19.	The yield of very thin PAMS shells is quite low	3-19
3-20.	When interior deposits are found on a PAMS shell mandrel, interior deposits are also found	3-19
3-21.	A PAMS shell mandrel dried at room temperature has no observable interior deposits	3-20
3-22.	Nearly all batches of PAMS shells dried at room temperature have no observable deposits	3-20
3-23.	Dimples or domes are invariably seen on D -GDP _{normal} shells after pyrolysis	3-22

3-24. Dimples or domes seen optically in **D-GDP_{normal}** shells are often detected by the Spheremapper 3-22

3-25. The Young’s Modulus of **D-GDP_{strong}** shells decreases at thinner walls 3-23

3-26. **D-GDP** shells made using deuterated benzene as precursor 3-24

3-27. Argon permeability decreases as shells age in air 3-25

3-28. The lower CH stretching absorption in the strong GDP 3-26

3-29. The individual absorption peaks within the aggregate peak provide clues 3-27

3-30. The normalized buckle strength increases 3-27

3-31. The oxygen uptake of strong and “normal” GDP coatings as a function of time 3-28

3-32. An overview of the polyimide coating system 3-29

3-33. Deposition of ODA and PMDA occurs inside the coating chamber 3-29

3-34. FTIR scans of a polyimide film pre-imidization and post-imidization deposited on a salt disc 3-30

3-35. PAMS shells being roll coated in a spinning pan inside the polyimide 3-30

3-36. Polyimide shells prepared at GA are indistinguishable from shells prepared at UR/LLE 3-31

3-37. Debris in the coating pan 3-31

3-38. Pressure controlled furnace for imidizing thinner walled shells 3-31

3-39. We routinely deliver multilayer capsules containing dopant-free GDP 3-33

3-40. An example of a capsule order sheet 3-35

3-41. The decomposable mandrel technique has become the primary polymer capsule production technique 3-36

3-42. PAMS mandrels must have uniform walls 3-37

3-43. A z-translation laser stage permits interferometric measurement of capsule layer thicknesses 3-37

3-44. The XRF system is used to measure the concentration of dopants in GDP shells 3-38

3-45. Capsule diameter and overall procedures are measured by optical microscopy 3-39

3-46. In step one of the GA process, doped GDP is deposited on decomposable PAMS shells 3-40

3-47. Glass shells made by the **Si-GDP** process cover a much broader diameter and wall thickness range 3-42

3-48.	This AFM Spheremapper power spectrum of a 2.2 mm diameter glass shell made by the Si-GDP process demonstrates that the shell has excellent low mode sphericity	3-43
3-49.	Wall thickness uniformity around a glass shell is excellent over the full size range	3-43
3-50.	The superior wall thickness uniformity of glass shells	3-44
3-51.	The peaks in the XRF spectrum of an argon filled Si-GDP prepared glass shell	3-45
3-52.	The dip and flip technique	3-46
3-53.	A hole was drilled through the rotor of a small 12-V dc motor	3-47
3-54.	A capsule immersed in a PVA/isopropanol/water solution	3-47
3-55.	Spinning the shell while it is withdrawn from a solution of PVA ...	3-47
3-56.	Drying tracks and vacuum chuck marks are apparent	3-48
3-57.	In the polishing apparatus, the balls are held between the grooves in the upper and lower brass plates	3-49
3-58.	Polishing a titanium ball resting on the outside of the upper plate ..	3-49
3-59.	Titanium grade 100 ball before and after polishing	3-50
3-60.	SEM examination of the surface finish of a titanium ball	3-50
3-61.	Line-out traces from the AFM Spheremapper	3-51
3-62.	Although the surface finish is improving with polishing	3-52
3-63.	A gold hohlraum with 25 μ m thick walls	3-52
3-64.	An aluminum mandrel that will be used to form a cocktail hohlraum	3-53
3-65.	A small truncated gold cone used as part of an ICF target component	3-53
3-66.	Square pure aluminum witness plates	3-54
3-67.	A small circular witness plate with a single step	3-54
3-68.	A circular copper mandrel with a gold coating	3-54
3-69.	A gold flyer plate	3-54
3-70.	One of a set of small gold tubes	3-55
3-71.	A copper mandrel which will be plated with gold to produce a halfraum	3-55
3-72.	The WYKO microscope image of the surface of the mandrel	3-56
3-73.	The surface of a copper disk coated with gold	3-56
3-74.	The WYKO image of the roughened region on the copper disk	3-57
3-75.	A SEM photomicrograph of the surface of a copper hohlraum mandrel	3-58
3-76.	SEM view of a Nd-Dy-Au layered cocktail structure	3-60
3-77.	The AES analysis of the layered cocktail sample	3-60

3-78. A flyer plate is launched when a laser beam is pulsed through the substrate 3-63

3-79. In this backlighter type target assembly, a 4.5 mm polymer capsules is supported in a gold coated hohlraum by two Formvar™ films 3-65

3-80. We assemble EOS targets which are fielded on both Saturn and Z machines 3-66

3-81. An EOS panel was characterized by taking multiple smaller scans and “stitching” them together 3-67

3-82. The foam structure on the left is produced by a commercial process 3-67

3-83. Each foam system has a range of densities and cell sizes 3-68

3-84. This deuterated DVB foam target was part of a series on Z this year 3-69

3-85. The disk on the left is CRF 3-69

3-86. These three SEM photomicrographs show a fresh fracture surface of a PS foam 3-70

3-87. Both pictures are of the same sphere before and after washing 3-70

3-88. We fabricated a foam with two Be markers 3-71

3-89. This EOS panel contains two silica aerogel foam disks 3-72

3-90. Targets shipped to NRL during FY01 3-74

3-91. NIKE target frame with polymer film target 3-74

3-92. Aluminum CTMs 3-75

3-93. For a NRL experiment, the ridges on a patterned polystyrene film had to be mounted parallel to the edges of the Nike target holder ... 3-75

3-94. March Instruments PX 250 Plasma Asher 3-76

3-95. This filament-heated crucible is part of a salt coater 3-76

3-96. This photomicrograph by interference microscopy shows the uniformity of a sine wave pattern 3-78

3-97. The evaporative coater is used primarily for aluminum or gold coatings 3-78

3-98. Sputter coating facility at Schafer 3-78

3-99. Rippled surface on RF foam 3-79

3-100. This SEM micrograph shows the cell size and structure of DVB foam 3-79

3-101. This AFM trace of a DVB foam cast at 70 mg/cm³ shows an average feature size of approximately 1.5 to 2.5 μm 3-79

3-102. Drawing of an EOS Target for NRL 3-80

3-103. EOS target consisting of a five-level aluminum plate 3-80

3-104. By positioning the fringes from this white light interferometer, focus position and therefore film thickness can be measured precisely 3-81

3-105.	Our Veeco RST-500 scanning surface profilometer is used to measure the surface of complex objects	3-81
3-106.	The scanning surface profilometer	3-82
3-107.	A Nike target is examined by imaging transmitted UV light	3-82
3-108.	Shadowgraph of a 125 μm layer inside of a 2 mm diameter 4 μm thick polymer capsule with a fill tube	3-84
3-109.	A uniform 100 μm thick HD layer formed near the triple point	3-86
3-110.	The result of the first attempt to replicate earlier IR enhanced layering results with D ₂ was clearly unacceptable	3-88
3-111.	Cross section of layering sphere with new IR injection scheme	3-88
3-112.	A DT layer formed by pure β layering	3-89
3-113.	A DT layer with 44 mW of IR	3-89
3-114.	The empty shell's lower right section magnified	3-89
3-115.	Schematic showing insertion of shell into a hohlraum	3-90
3-116.	Layout for one-beam IR injection	3-91
3-117.	A view through the LEH of an ice layer undergoing IR illumination in a hohlraum	3-91
3-118.	Drawing showing a cut away view of the modified hohlraum assembly	3-92
3-119.	D ₂ TS as of early July 2001	3-93
3-120.	Components micromachined at GA from copper and coated with gold were sent to LLNL	3-95
3-121.	Basic hohlraum containing a D ₂ filled capsule	3-96
3-122.	Complex indirect drive target	3-96
3-123.	Target types can be made more difficult by the addition of new features	3-97
3-124.	These targets for experiments at OMEGA require unusual angles ..	3-97
3-125.	CPL top section glove box with experimental apparatus shown inside	3-98
3-126.	CPL imaging system shown with cryostat	3-98
3-127.	Additional components of the CPL imaging system	3-100
3-128.	Close-up of the CPL layering sphere	3-100
3-129.	The raw accelerometer signal spectrum	3-101
3-130.	Quantix CCD image of a 1 mm spider fiber mounted plastic sphere	3-102
3-131.	Graph of the variation in centroid position of acquired images on the CCD array	3-102
3-132.	Images of 1 μm pinhole at three locations on the 1024 \times 1024 CCD array	3-104

3-133.	Graphs of a 1 μ m pinhole image and PSF as a function of image location on the 1024 \times 1024 CCD array	3-104
3-134.	Plots of the PSF FWHM as a function of camera shutter speed and cryostat operating condition	3-106
3-135.	Aspect ratio graph of the 1 μ m pinhole image data	3-106
3-136.	Schematic of the timing and interconnections of plastic capsule development tasks required to meet the needs of the NIF program .	3-109
3-137.	Operational schematic of the spheremapper/wallmapper device	3-110
3-138.	Graphs of the interference patterns returned by shells	3-111
3-139.	A plastic shell mounted on a rotating vacuum chuck	3-111
3-140.	XRF emission of a gold-coated sphere	3-112
3-141.	Configuration of the sample detector and x-ray beam is illustrated here	3-112
3-142.	The uniformity of the gold layer is determined by rotating the shell	3-113
3-143.	Gold XRF counts and measured with shells in different orientations	3-113
4-1.	Program organization chart	4-2

LIST OF TABLES

3-1.	Microshells on order as of March 9, 2001	3-34
3-2.	Total number of capsules delivered during FY01	3-36
3-3.	Specifications for a “typical” order	3-36
3-4.	PAMS removal in nitrogen atmosphere	3-41
3-5.	Conversion to glass in air	3-41
3-6.	Each foam system has specific attributes that are desirable	3-68
3-7.	List of the patterned substrates currently available at Schafer for casting	3-77
3-8.	Power adsorption measurements in the first capsule were completed	3-87